Global Journal of Engineering and Technology Advances
eISSN: 2582-5003
Cross Ref DOI: 10.30574/gjeta
Journal homepage: https://gjeta.com/

(REVIEW ARTICLE)

Check for updates

Effect of preheating substrates and process parameters on cladding track geometry fabricated by laser cladding

Quan Van Nguyen *, Hiep Xuan Dang and Hung Viet Dao

Faculty of Mechanical Engineering, Le Quy Don Technical University, 236 Hoang Quoc Viet, Bac Tu Liem, Hanoi, Vietnam, 100000.

Global Journal of Engineering and Technology Advances, 2024, 21(01), 073–086

Publication history: Received on 19 August 2024; revised on 28 September 2024; accepted on 01 October 2024

Article DOI: https://doi.org/10.30574/gjeta.2024.21.1.0180

Abstract

Laser cladding (LC) is an advanced technique used for repairing large-scale components, such as rotors and valves, in thermal power plants and steel rolling mills. This technology is designed to facilitate efficient repairs, minimize repair costs, conserve materials, reduce processing time, and ensure adequate dilution between the substrate material and the deposited coating, while also enhancing corrosion resistance. In this research, the effects of preheating substrates and input process parameters on the geometric accuracy of single-track deposits, as well as the microstructure composition of multi-track deposits, were investigated. The Taguchi method was used to design an L9 orthogonal experimental array. The impact of process parameters, including substrate temperature, laser power, and scanning speed, on the morphology of a single track (track width, height, penetration depth, and dilution) was evaluated through ANOVA statistical analysis. SS316L stainless steel, recognized for its wear resistance, was used as the deposition material. The findings reveal that substrate temperature is the most critical factor influencing the dilution of the coating. Additionally, the microstructure of the deposited layers were systematically analyzed.

Keywords: Laser cladding (LC); SS316L; Pre-heating substrate; Direct Laser Metal Deposition (DLMD)

1. Introduction

Laser cladding (LC) is a cutting-edge surface engineering technique that enhances the resistance of materials to high temperatures, corrosion, and wear through the application of a metallurgically bonded cladding layer. Conventional surface modification methods, including electrodeposition, vapor deposition (CVD/PVD), thermal spraying, and welding, have some inherent limitations [1, 2, 3]. These challenges involve the poor repeatability and control in electrodeposition, insufficient bonding strength in vapor deposition coatings, and the extensive heat-affected zone linked to thermal spraying, among other drawbacks. Laser cladding is considered a subset of additive manufacturing and is specifically categorized under Direct Laser Metal Deposition (DLMD) technology [4]. LC is also employed for the restoration of components that have sustained damage due to wear or corrosion. For example, many traditional machines in industries like thermal power plants and steel rolling mills suffer damage and corrosion in critical components such as rotor shafts, rolling mill shafts, and globe valves. These parts are typically large dimension and made from C45 steel. Laser cladding provides an effective solution for repairing and refurbishing these parts, optimizing material use, reducing repair costs, and shortening processing times. This technique enhances the durability and performance of industrial equipment. It ensures controlled dilution, reliable metallurgical bonding, fine-grained structure, and minimal heat-affected zones between the substrate and the coating, preserving the integrity and functionality of the repaired components. Due to its high process flexibility, laser cladding is suitable for large-scale component production, repair, and the deposition of functionally graded materials [1]. Laser cladding involves two

* Corresponding author: Quan Van Nguyen

material feeding methods: powder or wire. The powder method is more frequently used due to its advantages, including shallower penetration depth and improved surface quality.

The process is influenced by various parameters such as laser power, scanning speed, shielding gas flow rate, powder feeding rate, and laser spot diameter. These parameters affect the geometric characteristics of the clad track, including width, height, depth, and the heat-affected zone as described in figure 1(HAZ) . The HAZ geometry can influence lap joint quality and the microstructure of the coatings. A critical factor is the substrate temperature prior to coating, which significantly impacts adhesion, uniformity, and overall coating performance. If not optimized, the substrate temperature can result in poor bonding, defects, and reduced durability. Rapid heating and cooling during laser cladding can also introduce defects like cracks, pores, and thermal stress in the clad layer.

Another important geometric characteristic is dilution, as shown in figure 1, and is defined as follows [1].

$$\text{Dilution} = \frac{S_2}{S_1 + S_2} \qquad \ldots\ldots\ldots\ldots(1)$$

Where S_1 represents the raised area above the substrate (mm^2), S_2 represents the melted area below the substrate (mm^2).

In appropriate process parameters can result in poor metallurgical bonding between the clad track coating and the substrate, which is detrimental to multi-layer and multi-channel formations [5]. As a result, researchers have focused on studying the impact of laser cladding parameters on the geometry and properties of the clad track [6]. Liu and Kovacevic systematically studied the laser cladding parameters of Fe-based powder on ASTM A36 steel using a high-power direct diode laser. Their results indicate that laser power is the most significant factor affecting clad width [7]. Manjaiah, Chen, J. Sun, and T. Yu. analyzed the geometry, surface waviness, and microstructure of deposited 316L stainless steel, showing that scan speed and laser power have contrasting effects on track shape and geometry of bead [8]. Addition, the effects of preheating temperatures on different substrates have been studied, there is limited research on the impact of preheating temperatures on C45 substrates[9, 10, 11]. This is particularly important in the field of metal deposition for repair applications, where preheating the substrate before laser cladding plays a critical role. It effectively reduces the cooling rate, temperature gradient, and residual stress in the coating.

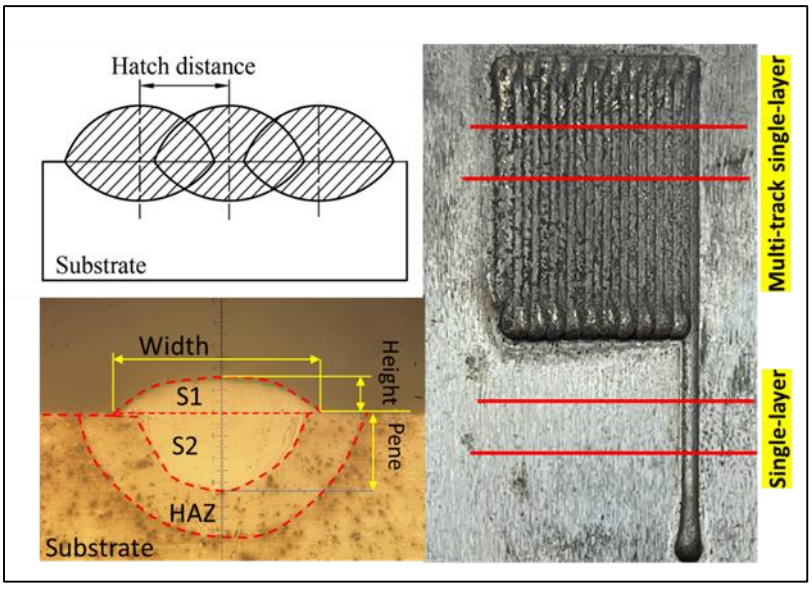

Figure 1 Model of single-track single-layer, multi-track single-layer

Austenitic stainless steel SS316L is particularly valuable in marine engineering, potable water systems, food preparation equipment, pharmaceutical manufacturing, and medical implants due to its excellent corrosion and oxidation resistance [12, 13, 14], high work hardening capacity, and good formability.

In this paper, the Taguchi method was employed using an L9 design of experiments (DOE) to study the influence of process parameters (temperature, laser power, scanning speed) on the responses (width, height, penetration and

dilution rate) in laser cladding of stainless steel SS316L powder. Additionally, the microstructure of the multilayered deposition was analyzed and evaluated the deposition layer material.

2. Materials and methods

2.1. Materials and the LC system

The LC system utilized in this study comprised of a 6.0 kW CO2 laser, a powder feeder, a deposition nozzle, and a three-axis CNC mechanism (Fig. 2a). The scanning electron microscope (SEM) and energy dispersive X-ray (EDX) analysis of morphology and element percentage composition data of the Stainless steel SS316L powder are shown in Figure 2 was used in the experiment.. The chemical composition is provided in Table 1. with particle sizes ranging from 15 to 45 µm, an average size of 21.171 µm, and a standard deviation of 6.3547µm (Figs. 2c and2d).

Table 1 Chemical composition of powder material (wt.%). SS316L

Powder SS316L	C (%)	Si (%)	Mn (%)	Cr (%)	Ni (%)	Mo (%)	Fe (%)
	0.02	0.42	0.76	18.4	11.4	2.19	64.69

In this work, the three C45 steel plate with a portion of the outer surface layer removed with dimensions of 200 x 60 x 10 mm were used as the substrate. Prior to coating, the substrates were sequentially polished with 200# and 400# waterproof abrasive paper, followed by cleaning with acetone and ethanol to remove grease and stains, thus eliminating the surface oxidation layer and improving surface quality. The SS316L powder was dried in a vacuum oven at 120 °C for 2 hours to remove moisture before laser cladding.

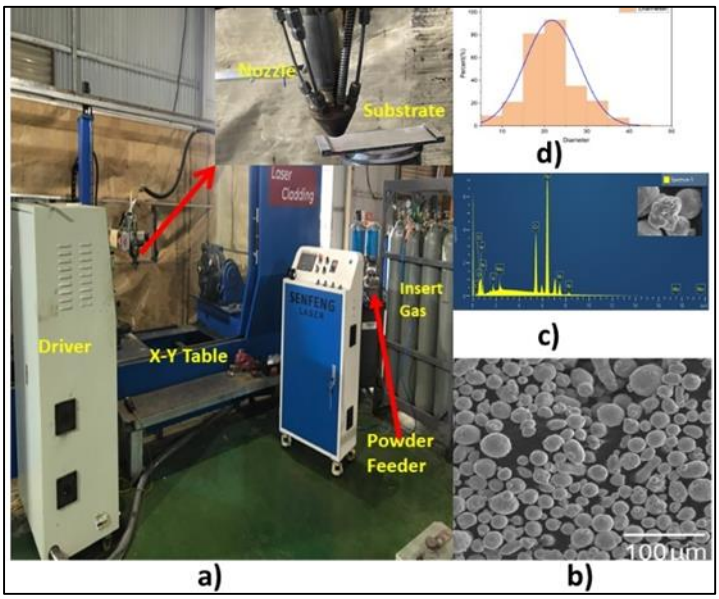

Figure 2 (a) The LC systems and (b) SS316L powder, (c)chemical composition of SS316L, (d)average size of SS316L

2.2. Fabrication of samples and data collection

In the LC process, various parameters influence the geometry and quality of the tracks. These include the laser beam spot diameter, the pressure and flow rate of the carrying/shielding gas, particle size distribution, laser power (P), powder feed rate (F), and nozzle scanning speed (S), among others [1, 2]. However, laser power and scanning speed are identified as the most critical factors, significantly impacting temperature distribution, melt pool dimensions, and track geometry [1]. Additionally, to evaluate the dilution of the deposition layer, the C45 substrate plate is heated. Figure 3 illustrates the key steps in the substrates plate heating process. Consequently, this research focuses on a parametric study of substrate heating (Temper), scanning speed (S), and laser power (P), while maintaining other parameters at fixed values

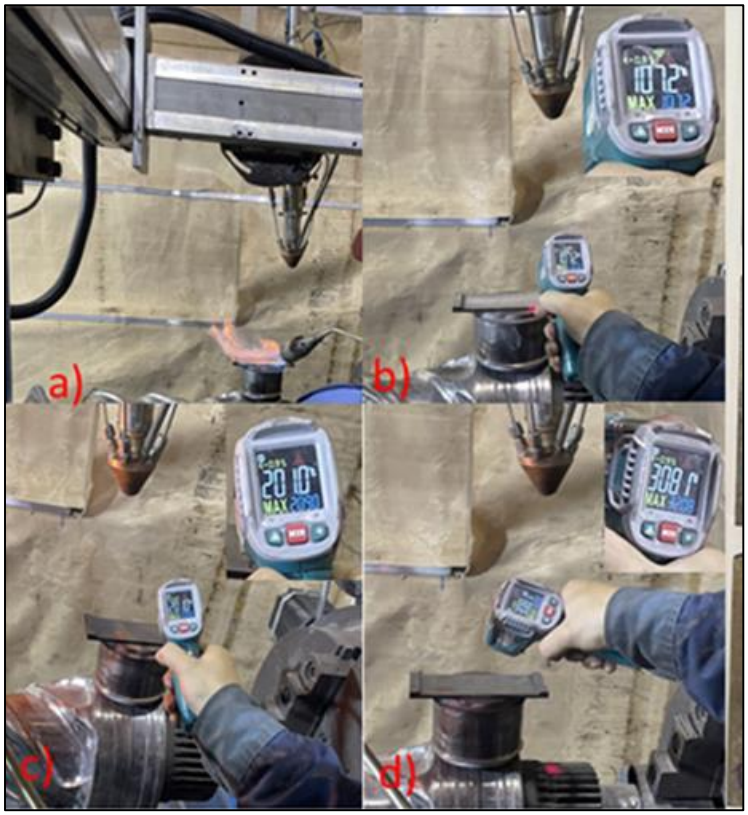

Figure 3 (a) preparation for heating; (b) heating at 100 °C; (c) heating at 200 °C; (d) heating at 300 °C

Table 2 Parameters and their levels utilized for LC

Variables	**Levels**		
	1	**2**	**3**
Temperature (^{0}C)	100	200	300
Power, P (W)	1000	1500	2000
Scan speed (mm/min)	1000	1200	1400

To fabricate the single deposited tracks, the experimental plan was structured using the L9 orthogonal array Taguchi method, assigning three levels to each parameter, as presented in Table 2. This resulted in a to a total of 9 experimental trials, which are listed in Table 3. Following deposition, the well-formed single tracks were cleaned, as illustrated in Figure 4. All depositions were carried out using an intermittent coaxial nozzle with argon as the shielding gas. The flow rates for both shielding and carrying gases were kept at 9 L/min, with a fixed nozzle-to-substrate distance of 15 mm and a laser beam spot diameter of 3 mm.

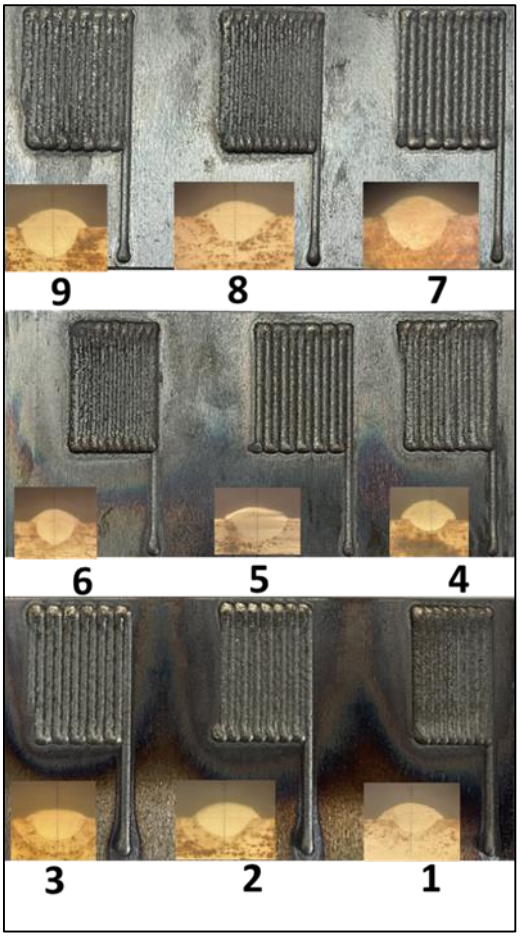

Figure 4 The result of single-track single-layer and multi-track single-layer

Table 3 Laser cladding matrix and responses

Runs	T (^{0}C)	P (W)	S (m/min)	Hatching (mm)	Height (mm)	Pene (mm)	S1 (mm^2)	S2 (mm^2)	Dilution (%)
1	100	1000	1000	1	0.493	0.422	0.629	0.379	37.60
2	100	1500	1200	1.5	0.455	0.548	0.634	0.394	38.33
3	100	2000	1400	2	0.481	0.667	0.8	0.542	40.39
4	200	1000	1200	2	0.45	0.388	0.869	0.543	38.46
5	200	1500	1400	1	0.474	0.76	0.552	0.465	45.72
6	200	2000	1000	1.5	0.535	0.757	0.54	0.803	59.79
7	300	1000	1400	1.5	0.419	0.541	0.611	0.604	49.71
8	300	1500	1000	2	0.517	0.654	0.428	0.62	59.16
9	300	2000	1200	1	0.55	0.856	0.667	0.985	59.62

It can be seen from the top view (Fig. 4) that all the single tracks are uniform and stable. Therefore, we can assume that these single grooves have nearly constant groove width and height values, especially in the middle region of each groove. Accordingly, the cross-sections of each single groove in the middle region were extracted, ground, polished, and chemically etched to measure the properties (w, h, p, S1, and S2). The measurements of w, h, and p were conducted

using an optical microscope (AXIO A2M, Carl Zeiss). The measurement results are presented in Table 3, the dilution is calculated using Equation (1). The measured data for the single grooves was used to analyze the influence of process variables on the attributes of the single deposited tracks.

Similarly, it was observed that the single-layer multi-tracks with a hatching distance of 1 mm (experiments 1, 5, and 9) exhibited smooth and well-formed surfaces. These single grooves were used to evaluate the microstructure.

3. Results and discussion

In this study, influence analysis models for individual track attributes (Width, Height, Penetration, and Dilution) were developed using Minitab 18 software. An analysis of variance (ANOVA) was performed for the models with a confidence level of 95% and a significance level of 5%.`

3.1. Effect of Process Parameters on Width

The influence analysis model for width (W) is expressed by Equation (2), and the ANOVA results for the Width model are presented in Table 4. The analysis shows that the model and all its terms {T, P, and S} are significant, with P-values less than 0.05. Among the process variables, scanning speed (S) contributes the most, accounting for 53.32%, followed by laser power (P), which contributes 34.76%. The contribution of temperature (T) is relatively minor, accounting for approximately 3%. Figure 5 illustrates the main effects of process parameters on width (W), showing that as nozzle traverse speed increases, the width (W) is significantly impacted by scanning speed (S), leading to a rapid reduction in width per unit of deposition length. Consequently, the bead geometry width decreases at higher traverse speeds.

$$\text{Width} = 2.134 + 0.000165\ \text{Temper(D)} + 0.000124\ \text{P(W)} - 0.000385\ \text{S(m/min)} \quad \ldots\ldots\ (2)$$

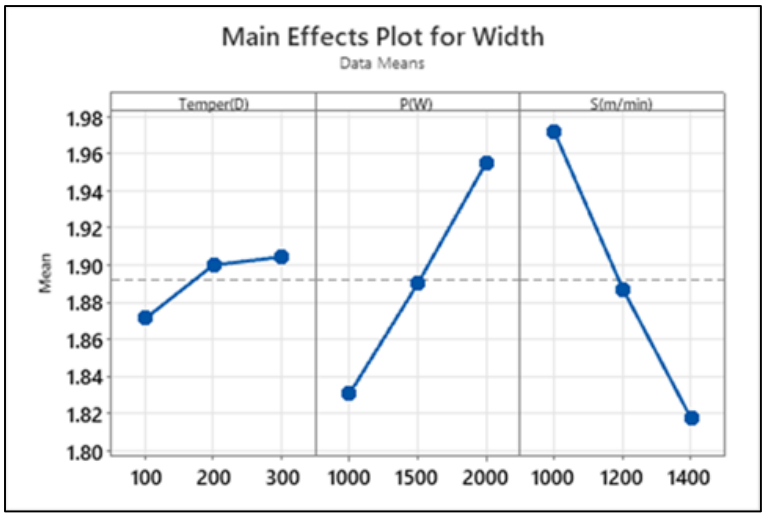

Figure 5 The influence of process parameters on the Width

Table 4 ANOVA results evaluating the influence of process parameters on Width (mm)

Source	DF	Seq SS	Contribution	Adj SS	F-Value	P-Value
Regression	3	0.060396	90.53%	0.060396	15.93	0.005
Temper (D)	1	0.001634	2.45%	0.001634	1.29	0.307
P(W)	1	0.023188	34.76%	0.023188	18.35	0.008
S(m/min)	1	0.035574	53.32%	0.035574	28.15	0.003
Error	5	0.006319	9.47%	0.006319		
Total	8	0.066715	100.00%			

Figure 6 illustrates the interaction effects of process parameters on the Width. Given the significant contribution of traverse speed to the width, it is evident that the width increases as the traverse speed decreases. In laser cladding processes, reducing the scanning speed (S) is crucial for maintaining the desired workpiece width.

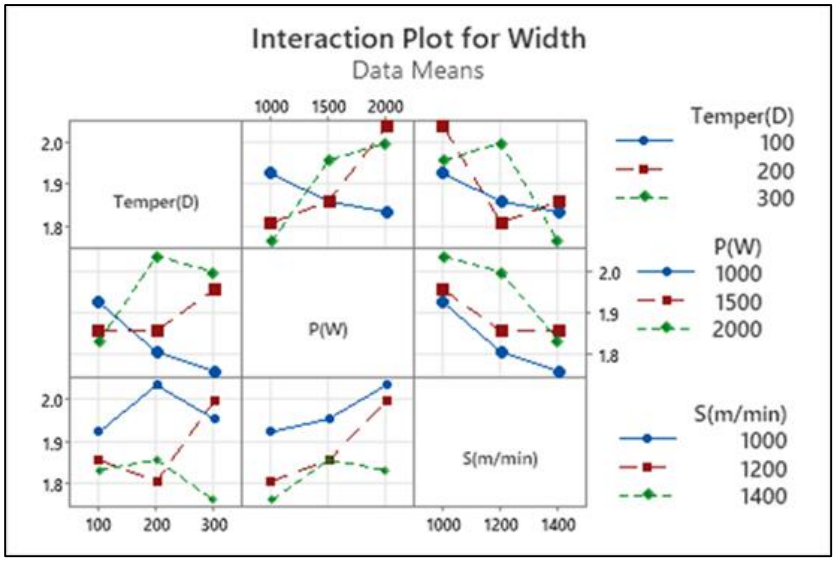

Figure 6 The interaction effects of process parameters on the Width

3.2. Effect of process parameter to Height (mm)

The influence analysis model for height (H) is described by Equation (3), with the ANOVA results provided in Table 5. The analysis shows that the model and all its terms { T, P, and S } are significant, with P-values below 0.05. In this model, laser power (P) has the largest contribution at 48.09%, followed by scanning speed (S) at 33.79%, while temperature makes a smaller contribution of 3.75% as described in figure 7.

$$\text{Height}=0.5360+ 0.000095\ \text{Temper(D)}+ 0.000068\ \text{P(W)}- 0.000143\ \text{S(m/min)} \quad \text{.....(3)}$$

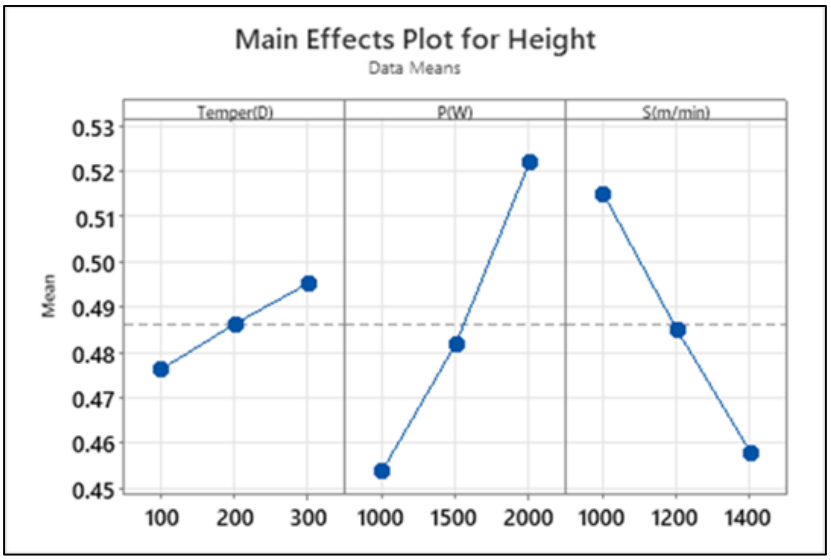

Figure 7 The influence of process parameters on the height of geometry bead

Table 5 ANOVA results evaluating the influence of process parameters on Height (mm)

Source	DF	Seq SS	Contribution	Adj SS	F-Value	P-Value
Regression	3	0.012351	85.64%	0.012351	9.94	0.015
Temper(D)	1	0.000542	3.75%	0.000542	1.31	0.305
P(W)	1	0.006936	48.09%	0.006936	16.75	0.009
S(m/min)	1	0.004874	33.79%	0.004874	11.77	0.019
Error	5	0.002071	14.36%	0.002071		
Total	8	0.014422	100.00%			

Figure 8 presents the interaction effects of process parameters on height. The results indicate that laser power exerts a significant influence on height, with an increase in height observed as laser power is elevated and scanning speed is reduced. In laser cladding, height enhancement is primarily achieved by increasing laser power (P) while decreasing scanning speed (S).

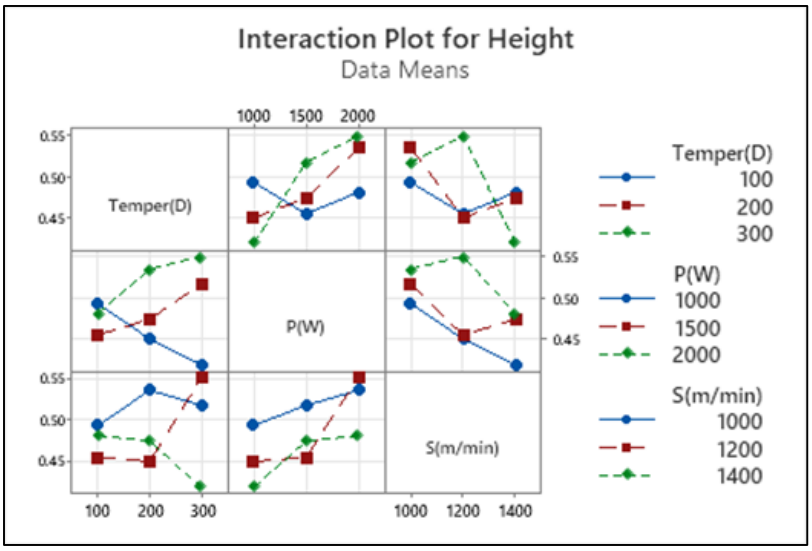

Figure 8 The interaction effects of process parameters on the height H (mm)

3.3. Effect of process parameter to Penetration (mm)

The effect on penetration is described by Equation (4), with the ANOVA results for the model presented in Table 6. The analysis indicates that the model and all its terms {T, P, S} are significant, as evidenced by P-values below 0.05. Among the process variables, laser power (P) has the greatest impact, contributing 71.26%, followed by temperature (T) at 14.15%. In contrast, scanning speed (S) has a relatively minor influence, contributing approximately 2%.

$$\text{Pene} = -0.116 + 0.000690\ \text{Temper(D)} + 0.000310\ \text{P(W)} + 0.000113\ \text{S(m/min)} \quad \ldots\ldots\ldots\ldots (4)$$

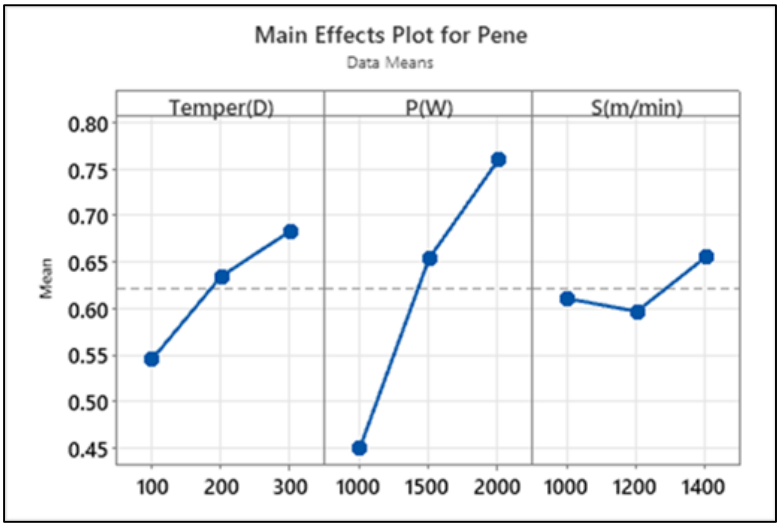

Figure 9 The influence of process parameters on the penetrationt of single track

Table 6 ANOVA results evaluating the influence of process parameters on Penetration (mm)

Source	DF	Seq SS	Contribution	Adj SS	F-Value	P-Value
Regression	3	0.175444	86.91%	0.175444	11.07	0.012
Temper(D)	1	0.028566	14.15%	0.028566	5.41	0.068
P(W)	1	0.143840	71.26%	0.143840	27.22	0.003
S(m/min)	1	0.003037	1.50%	0.003038	0.57	0.483
Error	5	0.026421	13.09%	0.026421		
Total	8	0.201864	100.00%			

Figure 10 shows the interaction effects of process parameters on penetration. The results indicate that laser power significantly affects penetration, with greater penetration observed as laser power and temperature increase. In laser cladding, penetration is primarily enhanced by simultaneously increasing both laser power (P) and temperature (T).

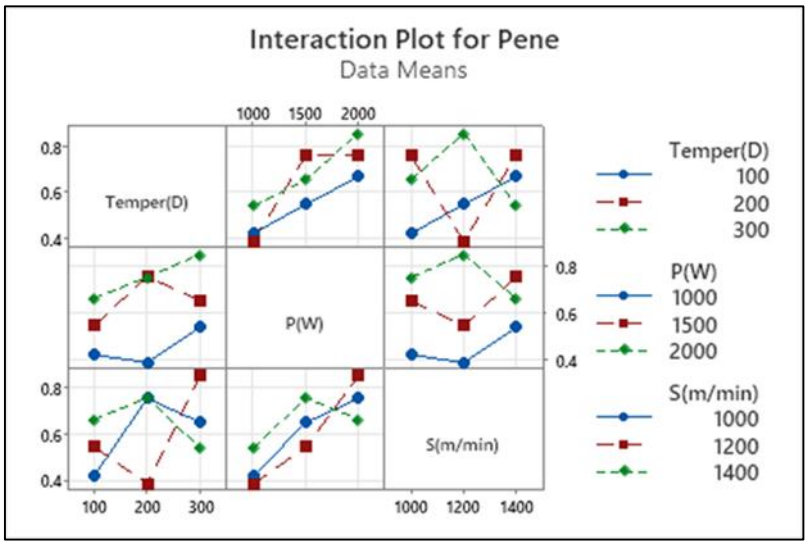

Figure 10 The interaction effects of process parameters on the Penetration (mm)

3.4. Effect of process parameter to Dillution (mm)

The impact analysis model for dilution is described by Equation (5), with the corresponding ANOVA results provided in Table 7. The analysis confirms that the model and its factors {T, P, S} are statistically significant, all showing P-values below the 0.05 threshold. Figures 10 and 11 illustrate the main and interaction effects of process parameters on the dilution of the deposited track. The data reveal a positive correlation between dilution and both substrate temperature (T), which increases from 100 °C to 300 °C, and laser power (P), which rises from 1000W to 2000W. Among the process parameters, substrate temperature has the greatest influence, contributing 60.00%, followed by laser power (P) at 25.53%, and scanning speed (S) at 9.46%. Figure 11 also shows that the effect of scanning speed on dilution exhibits non-linear behavior.

$$\text{Dilution} = 33.96 + 0.0870\ \text{Temper(D)} + 0.01134\ \text{P(W)} - 0.01727\ \text{S(m/min)} \quad \ldots\ldots\ldots\ldots (5)$$

This model underscores the significant impact of substrate temperature on dilution depth throughout the design space, providing valuable insights for laser cladding processes, particularly in the restoration of damaged components.

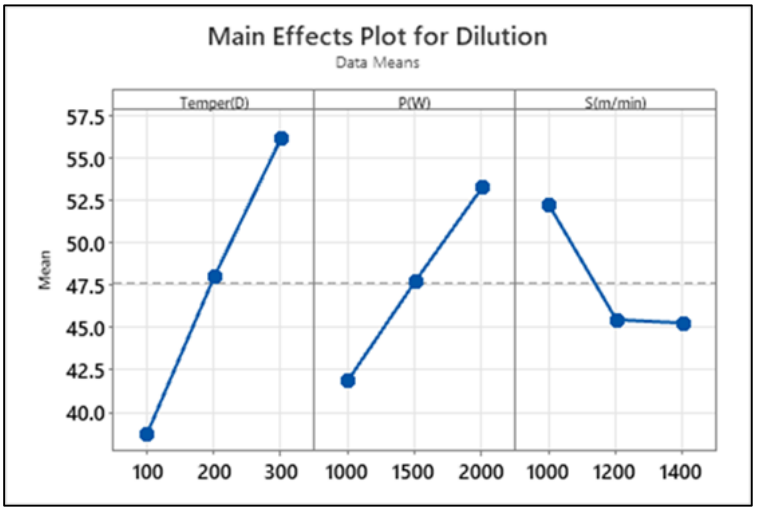

Figure 11 The influence of process parameters on the dilution of single track

Table 7 ANOVA results evaluating the influence of process parameters on Dilution

Source	DF	Seq SS	Contribution	Adj SS	F-Value	P-Value
Regression	3	718.39	94.99%	718.39	31.63	0.001
Temper(D)	1	453.76	60.00%	453.76	59.93	0.001
P(W)	1	193.06	25.53%	193.06	25.50	0.004
S(m/min)	1	71.57	9.46%	71.57	9.45	0.028
Error	5	37.86	5.01%	37.86		
Total	8	756.25	100.00%			

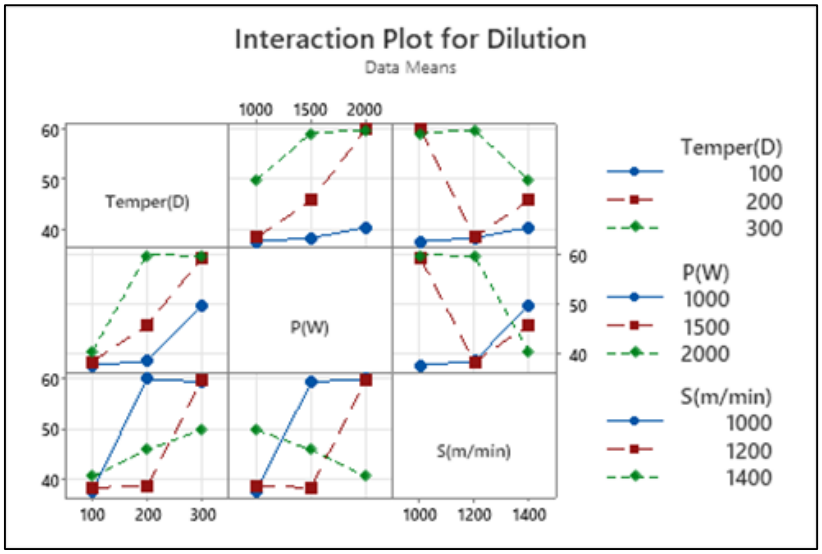

Figure 12 The interaction effects of process parameters on the height H (mm)

3.5. Microstructure

3.5.1. Microstructure of single track

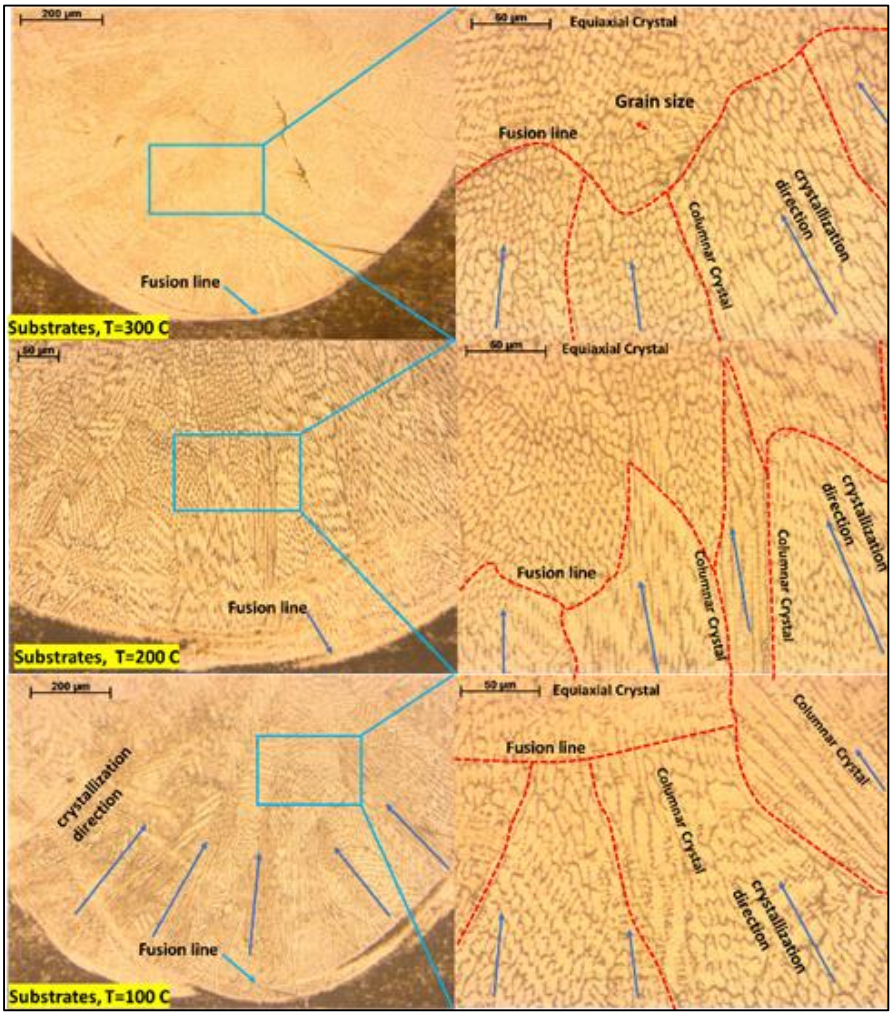

Figure 13 The microstructure of single track of Substrate 100 ^{0}C, 200 ^{0}C, 300 ^{0}C

Figure 13 illustrates the microstructure of the single deposited track on a pre-heated substrate at temperatures of 100 °C, 200 °C, and 300 °C. The growth direction and morphology of the grains are primarily determined by the crystallization parameter G/R (where G is the temperature gradient and R is the solidification rate) [15]. The growth direction of dendrites is opposite to the temperature gradient. Due to the significant temperature gradient at the top and bottom of the coating, the crystals exhibit a clear growth orientation, forming both columnar and equiaxed crystals. The growth orientation of these crystals in the middle of the coating is mainly governed by the direction of heat flow, which results in the grain growth shown in figure 13.

The microstructure of the substrate at 100 °C shows a mixture of columnar and equiaxed crystals with uneven grain distribution. Due to rapid cooling, the coating experiences a high degree of undercooling during the solidification process, leading to the formation of columnar crystals and some equiaxed crystals. In comparison, the grain structure of substrates at 200 °C and 300 °C becomes finer, more equiaxed, and contains a greater proportion of equiaxed crystals than columnar crystals, as illustrated in Figure 13.

3.5.2. Microstructure of multitrack, singe-layer

The cross-sectional morphology of the multi-track single-layer structures of samples 1 (substrates heated to 100 °C) and 9 (substrates heated to 300 °C) is shown in Fig. 14. The remelted or transition zone can be fully remelted, reducing defects caused by slag inclusions and incompletely melted particles in the overlapping region, thereby enhancing the quality of interlayer metallurgical bonding. An appropriately remelted area ensures that the powder at the edges of the clad track is completely remelted, facilitating strong metallurgical bonding in the overlap zone.

In the overlap region of substrates heated to 300 °C, equiaxed crystals predominantly form in the deposition area between layers. The columnar crystals in the metallurgical bonding area exhibit different orientations and are perpendicular to the substrate. In contrast, the microstructure of substrates heated to 100 °C is notably stratified in the overlapping area. Although columnar crystals still form in the metallurgical bonding area, their content, length, and overall size are greater than those observed at 300 °C. The boundary of the molten pool is characterized mainly by fine equiaxed crystals

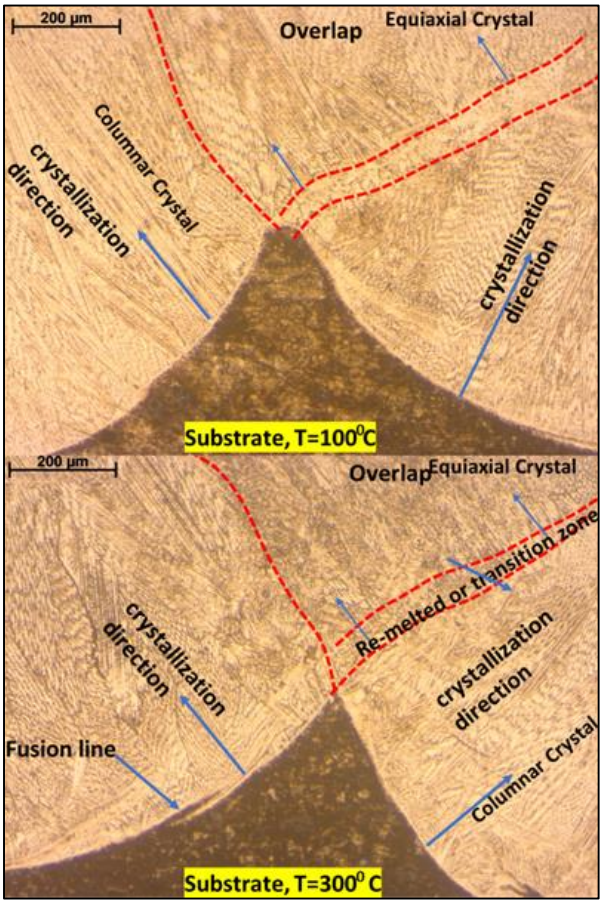

Figure 14 The microstructure of multi-track single-layer of Substrate 100 ⁰C, 300 ⁰C

4. Conclusions

In this study, the effects of key process variables—including substrate temperature (T), laser power (P), and cladding nozzle scanning speed (S)—on the characteristics of single deposited tracks in the laser cladding (LC) of SS316L, as well as the microstructure of multi-layer deposits, were thoroughly examined. Optimal process parameters for depositing SS316L structures were identified. The key findings of this research are summarized as follows:

Laser power (P) had the most significant influence on the deposited track height (H) and penetration (Pene), contributing 48.09% and 71.26%, respectively.

Scanning speed (S) had the greatest effect on the deposited track width (W), contributing 53.32%, and also significantly affected height, with a contribution of 33.79%.

Substrate temperature (T) primarily impacted dilution, contributing up to 60%.

Given the importance of single bead tracks in the laser cladding process, this research provides valuable insights into how primary process parameters affect single tracks, particularly substrate temperature, offering benefits for both academic research and industrial applications. However, to gain a more comprehensive understanding of the effects of process parameters on cladding, future studies should consider additional variables such as multi-layer and multi-track configurations, laser beam spot diameter, carrying/shielding gas pressure and flow rate, stand-off distance, and particle size

Compliance with ethical standards

Disclosure of conflict of interest

No conflict of interest to be disclosed.

References

[1] Y. Liu, Y. Ding, L. Yang, R. Sun, T. Zhang, and X. Yang, Research and progress of laser cladding on engineering alloys: A review, Jun. 01, 2021, Elsevier Ltd. doi: 10.1016/j.jmapro.2021.03.061.

[2] Y. Liang, Z. Y. Liao, L. L. Zhang, M. W. Cai, X. S. Wei, and J. Shen, A review on coatings deposited by extreme high-speed laser cladding: processes, materials, and properties, Sep. 01, 2023, Elsevier Ltd. doi: 10.1016/j.optlastec.2023.109472.

[3] S. Singh, D. K. Goyal, P. Kumar, and A. Bansal, Laser cladding technique for erosive wear applications: A review, 2020, Institute of Physics Publishing. doi: 10.1088/2053-1591/ab6894.

[4] K. Doan Tat, V. T. Le, and N. Duong Van, Prediction models and multi-objective optimization of the single deposited tracks in laser direct metal deposition of 316L stainless steel, Manuf Rev (Les Ulis), vol. 11, 2024, doi: 10.1051/mfreview/2024012.

[5] Y. Zhao, C. Guan, L. Chen, J. Sun, and T. Yu, Effect of process parameters on the cladding track geometry fabricated by laser cladding, Optik (Stuttg), vol. 223, Dec. 2020, doi: 10.1016/j.ijleo.2020.165447.

[6] Z. Xu, J. Yuan, M. Wu, A. F. M. Arif, and D. Li, Effect of laser cladding parameters on Inconel 718 coating performance and multi-parameter optimization, Opt Laser Technol, vol. 158, Feb. 2023, doi: 10.1016/j.optlastec.2022.108850.

[7] S. Liu and R. Kovacevic, Statistical analysis and optimization of processing parameters in high-power direct diode laser cladding, International Journal of Advanced Manufacturing Technology, vol. 74, no. 5–8, pp. 867–878, Sep. 2014, doi: 10.1007/s00170-014-6041-y.

[8] Y. Zhao, L. Chen, J. Sun, and T. Yu, Mechanical property of YCF101 coating under different overlap modes by laser cladding, Optik (Stuttg), vol. 212, Jun. 2020, doi: 10.1016/j.ijleo.2020.164714.

[9] C. Ding, X. Cui, J. Jiao, and P. Zhu, Effects of substrate preheating temperatures on the microstructure, properties, and residual stress of 12CrNi2 prepared by laser cladding deposition technique, Materials, vol. 11, no. 12, Nov. 2018, doi: 10.3390/ma11122401.

[10] Y. Liu, T. Xu, M. Yu, and G. Chen, Effect of substrate's preheating temperature on microstructure and properties of Ni-based alloy coatings. [Online]. Available: https://ssrn.com/abstract=4185978

[11] N. Panahi, M. Åsberg, C. Oikonomou, and P. Krakhmalev, Effect of preheating temperature on the porosity and microstructure of martensitic hot work tool steel manufactured with L-PBF, in Procedia CIRP, Elsevier B.V., 2022, pp. 166–170. doi: 10.1016/j.procir.2022.08.142.

[12] L. Song, G. Zeng, H. Xiao, X. Xiao, and S. Li, Repair of 304 stainless steel by laser cladding with 316L stainless steel powders followed by laser surface alloying with WC powders, J Manuf Process, vol. 24, pp. 116–124, Oct. 2016, doi: 10.1016/j.jmapro.2016.08.004.

[13] L. Gil, S. Brühl, L. Jiménez, O. Leon, R. Guevara, and M. H. Staia, Corrosion performance of the plasma nitrided 316L stainless steel, Surf Coat Technol, vol. 201, no. 7 SPEC. ISS., pp. 4424–4429, Dec. 2006, doi: 10.1016/j.surfcoat.2006.08.081.

[14] H. Ding et al., Optimization and wear behaviors of 316L stainless steel laser cladding on rail material, Wear, vol. 523, Jun. 2023, doi: 10.1016/j.wear.2023.204830.

[15] L. Chen, Y. Sun, L. Li, and X. Ren, Microstructure evolution, mechanical properties, and strengthening mechanism of TiC reinforced Inconel 625 nanocomposites fabricated by selective laser melting, Materials Science and Engineering: A, vol. 792, Aug. 2020, doi: 10.1016/j.msea.2020.139655.